Novel Organo-Functional Titanium−oxo-cluster-Based Hybrid Materials with Enhanced Thermomechanical and Thermal Properties

Sondes Trabelsi,*,† Andreas Janke,† Rüdiger Hässler,† Nikolaos E. Zafeiropoulos,*,† Giulia Fornasieri,‡ Sergio Bocchini,§ Laurence Rozes,‡ Manfred Stamm,† Jean-François Gérard,§ and Clément Sanchez‡

Department of Nanostructured Materials, Leibniz Institut für Polymerforschung Dresden e.V., Hohe Strasse 6, 01069 Dresden, Germany, Laboratoire de Chimie de la Matière Condensée, UMR CNRS 7574, Université Pierre et Marie Curie, 4 Place Jussieu, 75252 Paris Cedex, France, and Laboratoire des Matériaux Macromoléculaires/IMP UMR CNRS 5627, INSA de Lyon, 20 Avenue A. Einstein, 69621 Villeurbanne Cedex, France

Received April 7, 2005; Revised Manuscript Received May 16, 2005

ABSTRACT: Two novel nanomaterials based on hybrid organic−inorganic polymers have been prepared via free radical polymerization of (I) dimethacrylate oligomers and (II) 2-hydroxyethyl methacrylate (HEMA) in the presence of different contents of organically modified titanium−oxo-clusters $Ti_{16}O_{16}(OEt)_{24}(OC_2H_4Mc)_8$ (OMc = methacrylate). Investigations, combining small-angle X-ray scattering (SAXS), transmission electron microscopy (TEM), and energy-filtering transmission electron microscopy (EFTEM) lead to consistent structural and morphological characteristics for both grades of hybrid materials. Structural features, such as the subunit size and fractal dimensions are extracted from SAXS profiles. For the first grade of nanomaterials, i.e., for different content of titanium−oxo-clusters (2.5, 5 and 7.5 wt %) incorporated into a dimethacrylate-based matrix, aggregates with ramified mass fractal structures were found. Semiquantitative studies of TEM and EFTEM images revealed the presence of a uniform size distribution in the case of 2.5 wt % titanium cluster content with a typical size of 30 nm. A larger size distribution has been found for the 5 wt % and 7.5 wt % between 30 and 180 nm. For the second grade of nanomaterials, i.e., the 19.2 wt % of organically modified titanium clusters incorporated into poly(HEMA), compact and highly dense aggregates with a size distribution from a few nm up to 50 nm were found from TEM and EFTEM images. A significant increase of the storage modulus for the first grade of nanomaterials was revealed by dynamic mechanical analysis (DMA). The incorporation of Ti nanoclusters in the matrix lead to a significant alteration of the system's hardness as indicated through nano-indentation measurements. Thermogravimetric analysis also indicated a significant enhancement of the thermal stability compared to the neat matrix, probably because of the antioxidant effect of the titanium−oxo-clusters.

1. Introduction

Hybrid organic−inorganic materials offer great potential for high value-added applications (see ref 1 and references therein). Numerous hybrid organic−inorganic materials have been developed[2−6] using sol−gel chemistry, which enables the tailoring of the nanostructure of the inorganic component into a single hybrid nanocomposite.[7,8] The development of such multifunctional advanced materials has a major impact on future applications in diverse fields such as optics, electronics, ionic, mechanics, membranes, catalysis sensors, and biology. Existing hybrid materials have shown tuneable mechanical properties and improved optical and catalytic or membrane-based properties.[1,9] Phase segregation occurs during the preparation of nanocomposites because of the difficulty in controlling the reaction conditions, which define the size, shape, and monodispersity of the fillers inside the organic medium. The presence of covalent bonds or strong intermolecular interactions, e.g., hydrogen bonding, is a successful strategy to tackle the phase separation effect. A suitable approach to achieve a better control of the inorganic phase is to elaborate hybrids by assembling well-defined nano-building blocks (NBBs)[10−12] that maintain their integrity in the final material. NBBs (i.e., clusters, organically pre- or postfunctionalized nanoparticles and nanocore shells or layered compounds), which are properly functionalized, can be assembled without any damage into various types of structure to create new hybrid materials. It has been shown that the incorporation of organically modified silica particles or polyhedral oligomeric silsesquioxane (POSS) into dimethacrylate-based matrixes lead to an enhancement of mechanical properties such as fracture toughness,[13] as well as compressive and flexural strength.[14]

The oxo−alcoxo-cluster $Ti_{16}O_{16}(OEt)_{32}$ presents a shell of partially labile ethoxy groups that can be selectively transalcoholized with the preservation of the titanium oxocore, leading to new oxo−alcoxo-clusters $Ti_{16}O_{16}(OEt)_{32-x}(OR)_x$ (R: alkyl, phenyl, methacrylate, styrene, etc.). The reactivity of the $Ti_{16}O_{16}(OEt)_{32}$ cluster toward aliphatic and aromatic alcohols was recently reported. The reaction kinetics and the number of substituted titanium atoms depend strongly on the alcohol type and on the stoichiometric ratio used.[15] In the present study, the clusters are postfunctionalized with polymerizable ligands to connect them with the organic matrix through copolymerization. The transalcoholysis reaction was carried out by treatment of the oxo-cluster in a toluene solution with a strong excess of an aliphatic alcohol, the 2-hydroxylethyl-methacrylate ($H_2C{=}C(CH_3)CO_2CH_2$-

* Authors to whom correspondence should be addressed: trabelsi@ipfdd.de (S.T.); zafeiropoulos@ipfdd.de (N.E.Z.).
† Leibniz Institut für Polymerforschung Dresden e.V.
‡ Laboratoire de Chimie de la Matière Condensée.
§ Laboratoire des Matériaux Macromoléculaires/IMP.

10.1021/ma0507239 CCC: $30.25
Published on Web 06/11/2005

Table 1. Chemical Composition of Titanium-Based Materials Obtained from Titanium Clusters Incorporated into the Organic Matrix CD540/HEMA with a Weight Ratio of 2:1 and UV Cured for 108 s in Total in 9 Passages

			initiator		
sample name	CD540 g (wt %)	HEMA g (wt %)	type	g (wt %)	Ti cluster g (wt %)
UV_CDHEMA neat matrix	2.56 (62.0)	1.28 (31.0)	Darocur	0.16 (4.0)	
UV_Ti2.5	2.49 (62.3)	1.25 (31.2)	Darocur	0.16 (4.0)	0.10 (2.5)
UV_Ti5.0	2.43 (60.7)	1.21 (30.3)	Darocur	0.16 (4.0)	0.20 (5.0)
UV_Ti7.5	2.36 (59.0)	1.18 (29.5)	Darocur	0.16 (4.0)	0.30 (7.5)

Table 2. Chemical Composition of Titanium-Based Materials with High Concentration of Titanium Clusters Incorporated into Pure HEMA in Liquid State and UV Cured for 108 s in Total in 9 Passages

			initiator		
sample name	CD540 g (wt %)	HEMA g (wt %)	type	g (wt %)	Ti cluster g (wt %)
Sol_Ti19.2	0.00 (0.0)	3.07 (80.75)			0.77 (19.2)
UV_HEMA	0.00 (0.0)	3.84 (96.0)	Darocur	0.16 (4.0)	
UV_Ti19.2	0.00 (0.0)	3.07 (76.8)	Darocur	0.16 (4.0)	0.77 (19.2)

CH_2OH = HEMA). The modification with HEMA enables us to introduce eight methacrylate groups, leading to an octafunctional methacrylate cluster ($Ti_{16}O_{16}(OEt)_{24}(OC_2H_4Mc)_8$).[15,16] The functionalized clusters have been incorporated into two different grades of matrixes: (I) a dimethacrylate matrix and (II) poly(HEMA). The structure and morphology of the resulted nanohybrids as a function of the titanium cluster content, as well as the structural differences of titanium cluster aggregates formed in both types of matrixes, are discussed in the present article. The dynamic thermomechanical properties as well as thermal stability of type (I) hybrids depend on the titanium content incorporated inside the dimethacrylate matrix. Additionally, for hybrids based on the HEMA matrix, the influence of the UV curing process on the aggregate structure has also been investigated.

2. Experimental Section

2.1. Materials. Dimethacryloxy-tetraethoxylated bisphenol A (Figure 1a), denoted CD540, was purchased from Sartomer. 2-Hydroxyethyl methacrylate, denoted as HEMA 99% (Figure 1b) and azo-bis-isobutyronitrile, denoted as AIBN, were purchased from Sigma Aldrich. UV polymerization initiator Darocur 1173 was purchased from CIBA Vision. Tetraethoxyorthotitanate Ti$(OEt)_4$ was purchased from Fluka. All purchased materials have been used as received. The synthesis of the hybrid polymers proceeded in three steps. First, titanium clusters $Ti_{16}O_{16}(OEt)_{32}$ (Figure 1c) have been synthesized and functionalized with methacrylate ligands, producing an octafunctional titanium−oxo-cluster $Ti_{16}O_{16}(OEt)_{24}(OC_2H_4Mc)_8$ that was used for the preparation of the hybrid materials as described in details elswhere.[15] Three grades of hybrids were prepared, that differ from each other only in the following step.

(1) A set of samples was prepared by free radical polymerization of a CD540/HEMA mixture with a weight ratio of 2:1 in the presence of the nanoclusters. The comonomers, i.e., CD540 and HEMA, were first degassed under vacuum for at least 2 h and then mixed with three different solutions corresponding to 2.5, 5, and 7.5 wt % of clusters. After adding 4 wt % of Darocur 1173 under nitrogen atmosphere, the mixtures were brought into a 1 mm thick mould, and were subsequently UV-cured for 108 s in total, and in 9 passages under the UV lamp. Specimens termed as UV_Ti2.5, UV_Ti5, and UV_Ti7.5, with dimensions 30 × 5 × 1 mm^3 were obtained (Table 1). Additionally, one sample, termed as UV_CDHEMA, with only the neat organic matrix CD540/HEMA, has been prepared under similar conditions.

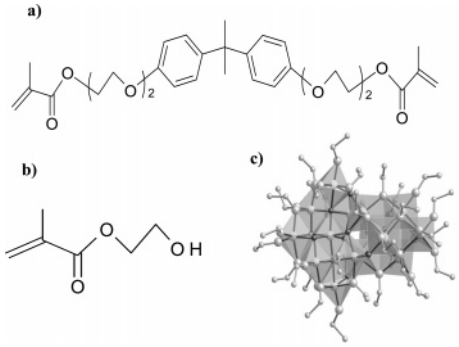

Figure 1. Representation of inorganic nano-building-block and organic monomers: (a) dimethacryloxy-diethoxy-bisphenol A (CD-540), (b) 2-hydroxyethyl methacrylate 99+% (HEMA), and (c) unmodified $Ti_{16}O_{16}(OEt)_{32}$ cluster.

(2) One sample, termed as UV_Ti19.2, has been prepared by bulk free radical polymerization of 2-hydroxyethyl methacylate (HEMA) in the presence of 19.2 wt % clusters. Additionally, the neat organic matrix poly(HEMA), termed UV_HEMA, has been also synthesized (Table 2). Both samples were prepared using the same UV curing process described above.

3) One solution, termed as Sol_Ti19.2, that contained 19.2 wt % of HEMA-modified nanoclusters incorporated simply in a solution of HEMA, has also been prepared (Table 2).

The HEMA monomer used in the present work may play a double role: (a) as organic ligands to functionalize the clusters and (b) as a reactive solvent to reduce the viscosity of the dimethacrylate monomer, thus facilitating the dispersion of the nanoclusters in the matrix. However, the incorporation of a high content of clusters (19.2 wt % in our case) could not lead to good level of dispersion for the mixture CD540/HEMA with a weight ratio of 2:1. Therefore, 19.2 wt % of HEMA-modified clusters have been incorporated only inside a neat matrix of poly(HEMA).

2.2. Experimental and Data Analyses. 2.2.1. Small-Angle X-ray Scattering (SAXS). Experimental Procedure. Small-angle X-ray scattering measurements were performed in transmission geometry using a homemade three-pinhole collimation system equipped

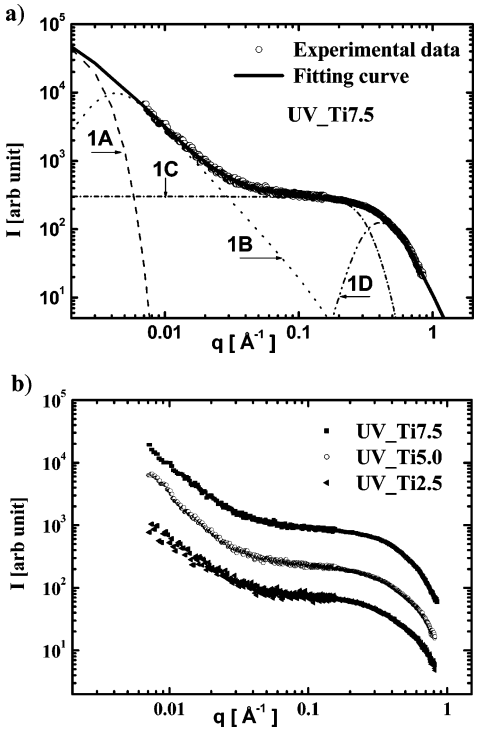

Figure 2. (a) Experimental SAXS profile $I(q)$ (open circle) and fitting curve (solid line) using the Beaucage model for the UV_Ti7.5 sample. The four contributions are represented by 1A (dashed), 1B (dotted line), 1C (short dash−dot), and 1D (dash−dot−dot). (b) Experimental SAXS profiles $I(q)$ of the UV_Ti2.5, UV_Ti5, and UV_Ti7.5 samples. The profiles are shifted vertically for clarity. $I(q)$ is the scattering intensity after normalization and subtraction of scattering contribution of the neat matrix UV_CDHEMA (cf. Section 2.2.1).

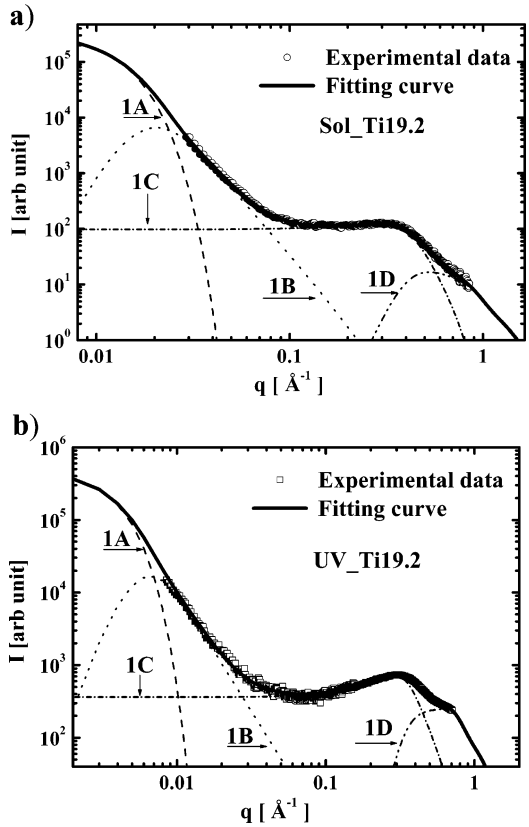

Figure 3. Experimental SAXS profiles I(q) (open circle) and fitting curves (solid line) using the Beaucage model for (a) Sol_Ti19.2 and (b) UV_Ti19.2 samples. $I(q)$ is the scattering intensity after normalization and subtraction of scattering contribution of the neat UV_HEMA (cf. Section 2.2.1).

with an Osmic multilayer mirror for higher photon flux at smaller beam spots, a Rigaku rotating anode generator (Cu Kα radiation $\lambda = 1.542$ Å, operating at 4.2 kW), and a HiStar 2D area detector (Bruker AXS). The scattering intensity has been recorded at two different sample-to-detector distances to cover a large scattering wave vector range ($q = 0.007-0.8$ Å^{-1}).

SAXS patterns were recorded for UV_CDHEMA, UV_Ti2.5, UV_Ti5, and UV_Ti7.5. All scattering patterns were first radially averaged to obtain the function $I(q)$ and then corrected for background scattering, X-ray absorption, and sample thickness variations. The scattering intensity $I(q)$ corresponding to the neat matrix (CD540/HEMA) has also been subtracted to determine the net scattering intensity of the titanium clusters shown in Figure 2. It should be noted that this correction does not alter the influence of the organic matrix on the structure of titanium cluster aggregates.

SAXS profiles have been recorded for Sol_Ti19.2 and UV_Ti19.2 samples. The same correction procedure mentioned above has been applied. However, the scattering profiles of pure HEMA in liquid state and of poly(HEMA) after UV curing (UV_HEMA) have been subtracted (Figure 3).

Data Analysis. Figures 2 and 3 show the scattering curves $I(q)$ in a log−log plot for both sets of samples {UV_Ti2.5, UV_Ti5, UV_Ti7.5} and {UV_Ti19.2, Sol_Ti19.2}, respectively. For two wave vector ranges 0.007 Å^{-1} < q < 0.015 Å^{-1} and 0.6 Å^{-1}< q < 0.8 Å^{-1}, the scattering intensity exhibits a power law decay. This power law decay has been argued to be linked to the fractal nature of scattering objects in the literature.[17−19] Fractals have been found to be very useful in describing many diverse phenomena in various fields of physical sciences.[20] However, as shown in Figure 2, these power law regimes display a structural limit, which appears as a sort of a plateau in the scattering profiles for the wave vector range 0.05 Å^{-1} < q < 0.6 Å^{-1}. A unified equation for the scattering intensity $I(q)$ has been proposed by Beaucage[17−19] to describe simultaneously the two mentioned regimes in the SAXS profiles (i.e., the power law decay and the plateau). In his model, one structural level pertains to a Guinier-like regime, describing an average structural size in terms of radius of gyration, and a structurally limited power law regime describing the mass, or surface fractal scaling for that level structure. It should be noted that the polydispersity effects have been neglected in this model. The Beaucage model is given in the following equations, and a full discussion of the model is be found in the literature.[18]

$$I(q) = G_1 \exp\left(-\frac{q^2 R_{g1}^2}{3}\right) \tag{1A}$$

$$+ B_1 \exp\left(-\frac{q^2 R_{g2}^2}{3}\right)\left[\frac{(\mathrm{erf}(qR_{g1}/\sqrt{6}))^3}{q}\right]^{p_1} \tag{1B}$$

$$+ G_2 \exp\left(-\frac{q^2 R_{g2}^2}{3}\right) S(q) \tag{1C}$$

$$+ B_2\left[\frac{(\mathrm{erf}(qR_{g2}/\sqrt{6}))^3}{q}\right]^{p_2} S(q) \tag{1D}$$

Table 3. Fitting Parameters of SAXS Profiles for Different Titanium Cluster Samples[a]

sample name	power law exponent large structure P_1	gyration radius R_{g2} [Å]	power law exponent small structure P_2	packing factor k	correlation distance d [Å]
UV_Ti2.5	2.17	6.50	4.00	0.74	17.5
UV_Ti5.0	2.42	6.88	4.00	0.80	18.0
UV_Ti7.5	2.10	7.13	4.00	0.98	18.2
UV_Ti19.2	3.26	5.31	4.00	2.84	16.5
Sol_Ti19.2	3.90	5.18	4.00	2.13	13.8
error bar	±0.05	±0.2	±0.05	±0.1	±0.5

[a] The general semiempirical model of Beaucage was applied for two structural levels and weakly correlated system given by eq 4.

where G_1 and G_2 are the Guinier pre-factors, R_{g1} and R_{g2} are the gyration radii, B_1 and B_2 the pre-factors of the fractal domains, erf(x) the error function. The indices 1 and 2 refer to a large-scale structure length and the titanium cluster as a subunit length scale, respectively. P_1 and P_2 are referred to as the Porod exponents.[21] To reduce the number of free parameters in eq 4, a relation between the power law factor B_1 and the Guinier pre-factor G_1, termed "polymeric constraint", has been used for the case of an arbitrary polymeric mass fractal:[19]

$$B_1 = \left(\frac{G_1 d_{f1}}{R_{g1}^{d_{f1}}}\right)\Gamma(d_{f1}/2) \tag{2}$$

where $d_{f1} = P_1 \leq 3$ is the fractal dimension of the mass fractal, $\Gamma(x)$ is the gamma function and R_{g1} is the radius of gyration. Generally, the power law exponent for a mass fractal lies between $1 \leq P \leq 3$ and for a surface fractal between $3 \leq P \leq 4$. The fractal dimension for a mass fractal structure corresponds to the power law exponent $d_f = P$, while for a surface fractal, the surface fractal dimension $d_{fs} = 6 - P$.[17,22] Beaucage et al.[23] also proposed a function for the structure factor $S(q)$ to account for particle−particle interference on the basis of the Born−Green theory[24] to describe the correlation of spherical colloidal particles or domains in terms of a correlation distance d and a packing factor k as:

$$S(q) = \frac{1}{1 + k\theta(q)} \tag{3}$$

where $\theta(q)$ is the form factor for structural correlations between particles:

$$\theta(q) = 3\frac{\sin(qd) - qd\cos(qd)}{(qd)^3} \tag{4}$$

where d corresponds to the average particle distance. The structure factor $S(q)$ (i.e., interference factor) was determined on the assumption of the interaction potential of hard-core spheres.[25−27] The set of eqs 1−4 was used to fit the experimental SAXS curves in the present study. All data fitting in the present study was carried out using the Mathematica 4.2 software package.

2.2.2. Transmission Electron Microscopy (TEM) and Energy-Filtering Transmission Electron Microscopy (EFTEM). Bright field TEM micrographs, both conventional and with energy-filtering, were taken from ultramicrotomed thin sections of UV_Ti2.5, UV_Ti5, UV_Ti7.5, and UV_Ti19.2 samples using an electron microscope EM 912 (Zeiss, Germany) operating at 120 kV. The slices of about 100 nm thickness were mounted on amorphous carbon-coated copper TEM grids. Energy-filtered images were recorded at an energy loss of $\Delta E = 250$ eV above the adsorption edge of titanium (Ti-$M_{2,3}$, 40 eV) and below that of carbon (C−K, 284 eV) optimized for the titanium contrast.

2.2.3. Nano-indentation for Hardness Assessment. Nano-indentation was carried out on UV_CDHEMA and UV_Ti2.5 samples with the AFM mentioned above. A Berkovich indenter probe, consisting of a diamond tip with a radius below 25 nm, mounted to a metal foil cantilever was used to indent the surface. To compare only qualitatively the hardness of the pure matrix with the matrix containing 2.5 wt % of clusters, an identical trigger threshold of 2.5 V was applied for both samples. We recall here that the trigger threshold is the cantilever deflection at which the controller stops pushing the tip into the surface. It is a measure also of the force applied on the sample during indentation. An array of four indents equidistant by 500 nm was carried out at four different places in both samples, with the same trigger threshold value and under the same indentation parameters. Height images of indents were recorded using the same diamond tip in tapping mode for UV_CDHEMA and UV_Ti2.5. To compare easily between the indents of UV_CDHEMA and UV_Ti2.5, we show only the height images of one indent for each material with comparable scan size of 507 × 507 nm^2 (Figure 7).

2.2.4. Dynamic Mechanical Thermal and Thermogravimetric Analyses. Dynamic mechanical thermal analysis (DMTA) was performed using a DMA 2980, TA Instruments (USA), in a single cantilever-deformation mode. Viscoelastic properties were determined on thin films with dimensions of 10 × 8 × 2 mm^3, applying a fixed amplitude deformation of 20 μm at a frequency of 1 Hz. Temperature scans from −100 °C to +200 °C with a heating rate of 2 K/min were applied.

Thermogravimetric analysis (TGA) was conducted with a Q500, TA Instruments (USA), under nitrogen and air atmospheres from room temperature up to 700 °C. The employed heating rate was 10 K/min.

3. Results and Discussion

3.1. Structure Characterization of Hybrid Nanomaterials. 3.1.1. Description of SAXS Profiles of Titanium Cluster with the Beaucage Model. Figure 2a shows the experimental scattering profile for the UV_Ti7.5 sample over the wave vector range 0.007 $Å^{-1} < q < 0.8$ $Å^{-1}$ as a typical example of the data fitting. The Beaucage model is used with a breakdown of the different profiles corresponding to the four terms expressed by eqs 1A, 1B, 1C, and 1D and the complete fitted curve of the model (solid line) is shown. All parameters derived from the fitting of the different samples are summarized in Table 3. The experimental scattering data was limited to the wave vector range 0.007 $Å^{-1} < q < 0.8$ $Å^{-1}$. Because of the minimum wave vector q_{min} imposed by the beam stop, there were not sufficient data points for an accurate determination of

the scattering profile of the large structures (i.e., low q), described by expression (1A), and hence, these results from the model were chosen to not be considered for the determination of the gyration radius R_{g1} (dashed line in Figure 2a). Therefore, we discuss here only the role of the contributions (1B), (1C), and (1D). The large-scale structures, described by expression (1B), are composed by small-scale structures captured by the terms (1C) and (1D).

For the wave vector range 0.007 $Å^{-1} < q < 0.015$ $Å^{-1}$, the contribution of (1B) dominates (dotted line in Figure 2a). It describes the power law decay of the scattering intensity $I(q)$ due to large structures defined by R_{g1}. This decay depends on the morphology of the large structure (P_1, R_{g1}) and on the size of the small structure R_{g2}. Therefore, for two interrelated structural levels, the power law decay ($-P_1$) cannot be accurately determined simply from the slope of the log−log plot, as already pointed out in a previous study by Beaucage.[18] The curves (1B) in Figures 2 and 3 describe well the scattering intensity decay for all cluster concentrations.

The expression (1C) is the predominant contribution in the wave vector range 0.07 $Å^{-1} < q < 0.4$ $Å^{-1}$. It describes the plateau like behavior and also the subunit−subunit interference effects that lead to a correlation peak (weak and almost unnoticeable for the low content of Ti systems, but strong and well-defined for the high Ti content hybrids) in the scattering profile (short dash−dot line in Figures 2 and 3). This curve represents also the cutoff of the power law given by (1B), which arises from a morphology transition from the large-scale to the small-scale structure of subunit particles with a gyration radius R_{g2}. We found correlation effects between the subunits of the formed aggregates, even for the lowest titanium cluster content of 2.5 wt % (Table 3), after fitting the Beaucage model on the experimental data. Correlation phenomena and related parameters (k, d) for the different titanium contents will be discussed in detail in Sections 3.1.3 and 3.1.4.

The second power law exponent P_2 and the gyration radius R_{g2} were determined in the wave vector range 0.4 $Å^{-1} < q < 0.8$ $Å^{-1}$ from the curve defined by expression (1D) (dash−dot−dot line in Figure 2a). It also covers partially the correlation broad peak in the wave vector range 0.4 $Å^{-1} < q < 0.6$ $Å^{-1}$. P_2 was found to be 4, indicating the presence of subunits with smooth surfaces and sharp interfaces with their surroundings, following the well-known Porod law[28] (Table 3). On the basis of the discussed data above, one may conclude that the Beaucage model is well-suited to describe the experimental SAXS scattering patterns over the whole wave vector range in our systems (Figures 2, 3). The interpretation of the structural parameters extracted from the fitting procedure is discussed in the following section.

3.1.2. Growth Process of Titanium Cluster Aggregates in Dimethacrylate-Based Matrixes. The power law exponent of the large structure $P_1 = 2.1$, determined from the SAXS data, indicates that the titanium clusters are mass fractals. The fractal dimension d_{f1} of these aggregates is given by $d_{f1} = P_1 = 2.1$. It has been found that there exists a slight fluctuation (albeit statistically significant) on the order of 0.3 in the fractal dimension values by increasing the titanium content (Table 3). Computer simulations of fractal aggregates, such as the one reported by Schaefer,[22] may turn out to be very useful to obtain a better insight into the internal structure and to describe the aggregation growth processes. Such simulations make use of assumptions concerning transport phenomena, such as diffusion and accretion. The possibilities for accretion include monomer-to-monomer (MM), monomer-to-cluster (MC), and cluster-to-cluster (CC) aggregation. The transport phenomena on the other hand, can be either diffusion or reaction collision limited aggregation. The fractal dimension $d_{f1} = 2.1$ of the titanium cluster aggregates derived from the data fits in the present study (Table 3) corresponds to a fractal dimension determined by simulations for reaction limited cluster−cluster (CC) aggregation (RLCA) that was carried out by Lin et al.[29] On the basis of the study of Lin et al. and the SAXS experimental data, the growth process (i.e., the aggregation process) of the titanium clusters in our system proceeds through collisions that take place because of cluster Brownian motion and result in the formation of larger aggregates of clusters after a large number of collisions. The formed clusters themselves continue to diffuse, collide, and form even larger clusters. The underlying growth process plays a very crucial role for the final value of the fractal dimension. Furthermore, following monomer−monomer (MM) and monomer−cluster (MC) aggregation processes, the resulting aggregates display fractal dimensions $d_f > 2.5$.[22] The formation of aggregates proceeds through the diffusion of single particles, while the growing aggregates remain stationary. Our SAXS experiments for the different titanium contents (2.5, 5, and 7.5 wt %) suggest that large aggregates having ramified and "open" structures are formed. The power law exponent $P_2 = 4$ indicates the presence of subunits with sharp interfaces. Assuming that these subunits are spherical, their radius is given by $R_0 = \sqrt{5/3}R_{g2}$, and thus their size (diameter) varies from 16.9 to 18.5 Å as the titanium content increases from 2.5 to 7.5 wt %. Each subunit corresponds probably to a single titanium cluster of dimension 12 × 17 $Å^2$, as has already been measured by Mosset et al.[30] by means of crystallography for the nonmodified titanium clusters.

3.1.3 Effect of Increasing the Titanium Content in Dimethacrylate-Based Matrixes. The degree of correlation occurring between the subunits of the titanium cluster aggregate is mainly defined by two parameters: (i) the average correlation distance denoted d, which is approximately two times the radius of the subunits ($d \approx 2R_0 \approx 18$ Å), and (ii) the packing factor $k = 8v_0/v_1$, where $v_0 = (4\pi/3)R_{g2}^3$ is the volume of a primary cluster or subunit, assumed to be a sphere, and $v_1 = V/N$ is the average volume provided to each subunit, with V being the total volume provided to N particles.

As seen in Table 3, R_{g2} and consequently v_0 of the subunit remains practically constant with the increase of the titanium content from 2.5 to 7.5 wt %, while the packing factor increases only slightly from 0.74 to 0.98. The variation of the packing factor can be explained by a simultaneous increase of the total volume V and the number N of subunits per aggregate, while the ratio V/N remains almost unchanged. Furthermore, fractal dimensions determined for UV_Ti2.5, UV_Ti5, and UV_Ti7.5 samples ($d_f = P_1 < 2.5$) confirm that titanium clusters are present as aggregates with ramified structure rather than being compact.

3.1.4. Structure of Titanium Clusters in HEMA-Based Matrixes. Compared to the previous nanoma-

terials, in which the organic phase, i.e., the matrix based on dimethacrylate monomer, is a highly cross-linked polymer,[31,32] in this part, the organic phase poly(HEMA) forms a slightly cross-linked polymer matrix because of the presence of a small percentage of ethylene glygol dimethacrylate (EGDMA). If one compares the scattering profiles of hybrids based on HEMA in the presence of 19.2 wt % titanium clusters before (Sol_Ti19.2, Figure 3a) and after the curing process (UV_Ti19.2, Figure 3b), one may see a remarkable change in the titanium cluster structure that occurred after curing. A power law exponent of $P_1 = 3.9$ for the aggregates formed in Sol_Ti19.2 sample has been found, indicating the presence of compact aggregates with small fractality. On the other hand, in the fully cured nanomaterials, compact aggregates with a much higher fractality formed ($P_1 = 3.26$).[17] Moreover, after curing interference effects between the subunits of the aggregates are more accentuated, leading to a visible correlation peak in SAXS profile (Figures 3b), and resulting in an increase of the packing factor from $k = 2.12$ for Sol_Ti19.2 to $k = 2.84$ for UV_Ti19.2. In other words, the gelation and immobilization of the HEMA polymer chains at fixed positions lead also to a firm placement of the titanium clusters at specific positions in the network. This implies an increase in the short-range order in terms of the correlation distance from $d = 13.8$ Å for Sol_Ti19.2 to $d = 16.5$ Å for UV_Ti19.2.

3.1.5. Small-angle Scattering of the Neat Matrixes. Because the matrix itself can be considered as one structural level, P has been derived simply from the slope of $I(q)$ in the log−log plot. Amorphous random polymer structures are usually classified as mass fractal structures through SAXS experiments with a fractal dimension of the order of $d_f = 2$.[33] Surprisingly, the scattering intensity in the wave vector range $0.007\ \text{Å}^{-1} < q < 0.015\ \text{Å}^{-1}$ of dimethacrylate-based matrix UV_CDHEMA display a power law decay of $P = -4.16$ (Figure 4a) and of $P = -4.28$ for the poly(HEMA) UV_HEMA (Figure 4b). These values indicate that these organic matrixes behave as systems of "particles" having a diffuse interface with the rest of the system. Indeed, such nanostructure has been previously reported by Rey et al.[34,35] for cross-linked networks of dimethacrylate matrixes (CD540) through dynamic light scattering (DLS) experiments, and attributed to the formation of domains with high cross-link density in comparison to the rest of the matrix. Dusek et al.[36] have also observed a nodular structure by scanning electron microscopy (SEM) on fractured surfaces of un-cross-linked polymers, such as poly(methyl methacrylate), which could probably be attributed in the formation of a heterogeneous network of physical cross-links, though the exact explanation of the phenomenon is still not well established. The SAXS analysis of both matrixes used in the present study does not reveal any difference in the scattering behavior, apart from the differences in the power law decay. Both materials display a heterogeneous structure, consisting of phases (probably of nodular structure) having a diffuse interface.

It should be noted that the growth process of the titanium aggregates depends strongly on the influence of the nature of the initial monomer and/or microstructure of the final polymer (UV_CDHEMA and UV_HEMA), i.e., the interactions between the inorganic and organic components. Compared to the HEMA-based matrix, the vitrification of the polymer matrix occurs more rapidly during the polymerization process of UV_CDHEMA, leading not only to a high cross-link density, but also to a more heterogeneous system. It is the interplay between these parameters that control and influence the mechanism of aggregation in the two systems, and since the UV_CDHEMA matrix reaches the vitrification state at a much faster rate, the phase segregation of the nanoclusters is severely disrupted, hence, leading to more ramified and open structures than in the case of the UV_HEMA matrix where the reaction proceeds at a much lower speed.

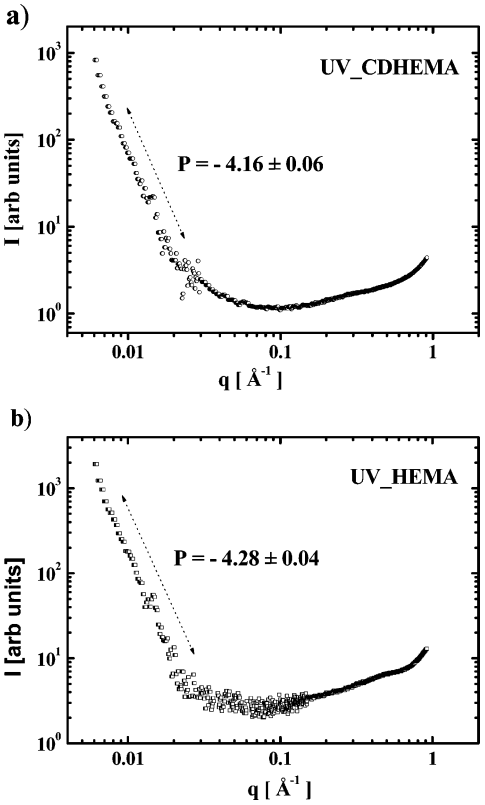

Figure 4. Normalized experimental SAXS profiles $I(q)$ of the neat organic matrix (a) UV_CDHEMA (open circle) used for normalization of the UV_Ti2.5, UV_Ti5, and UV_Ti7.5 samples and (b) UV_HEMA (open square) used for UV_Ti19.2. P is determined directly from the slope of $I(q)$ in the log−log plot.

3.2. Size and Distribution of Modified Titanium Clusters in Hybrid Nanomaterials. Conventional bright field TEM and energy-filtered images have been performed for UV_Ti2.5, UV_Ti5, UV_Ti7.5, and UV_Ti19.2. To obtain higher spatial resolution and sharp contrast, an energy filter value of 250 eV was chosen as follows: an electron energy loss spectrum (EELS) was measured only for the UV_Ti19.2 sample. The characteristic adsorption edges of the sample were the C−K edge (284 eV), the Ti-$M_{2,3}$ edge (40 eV), and the Ti-$L_{2,3}$ edge (455 eV). Elemental mapping images recorded at the Ti-L edge and the energy filtered image at different values of energy loss (at Ti-M edge, above the Ti-M edge and far below the C−K edge) revealed the same features. The brighter regions visible in the energy-filtered images consist only of titanium-rich domains because no other element with a characteristic energy loss in this range is present in the system. Furthermore, for an energy filter value of 250 eV, the additional undesirable contrast due to sample thickness variations could be successfully minimized. As an example, Figures 5a and 5b show the bright field TEM

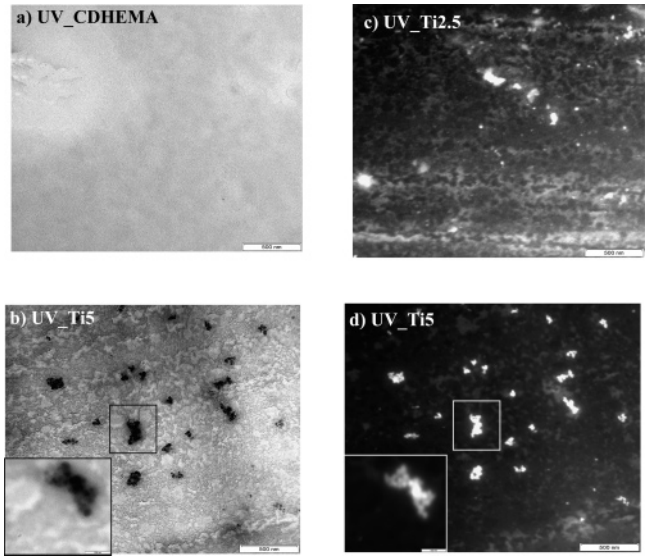

Figure 5. (a) Bright field TEM image of UV_CDHEMA. (b) Bright field TEM image of UV_Ti5 and (c) filtered energy TEM images of UV_Ti2.5. (d) Filtered energy TEM images of UV_Ti5. The large images have a bar scale of 500 nm, and the insets of 100 nm.

images of the neat matrix UV_CDHEMA and UV_Ti5. It should be underlined that the light and gray regions displayed by the bright field TEM and energy-filtered TEM images corresponds simply to the structure of the carbon-film-coated Cu TEM grids and not to the inherent features of the samples. The black domains in the bright field TEM image (Figure 5b) and the corresponding shining white domains in the energy-filtered TEM image (Figure 5d) of UV_Ti5 both represent the same titanium cluster aggregates. The insets of the TEM micrographs show some of the titanium cluster aggregates in higher magnification. As seen in the micrographs, the clusters are aggregating into ramified rather than into compact structures. The results from the TEM are in excellent agreement with the results from the SAXS measurements ($P_1 = 2.4$) that predict a similar structure for the Ti aggregates. Figures 5c and 5d illustrate the energy filtered images of UV_Ti2.5 and UV_Ti5. The increase of titanium content from 2.5 to 5 wt % leads to a visible reduction in the number and the size of aggregates as they appear as small, very sharp white spots (Figure 5c). The typical size of these small aggregates has been estimated to be approximately 30 nm, but it appears that there is a bimodal distribution with larger-size aggregates (albeit few with sizes between 80 and 180 nm) also present. The energy filtered micrograph of the UV_Ti5 (Figure 5d) and UV_Ti7.5 (not shown here) indicate the presence of a size distribution between 30 and 180 nm, and only very few smaller-size aggregates may be seen (of the order of 30 nm). It may thus be concluded, that in the UV_Ti2.5, with the exception of a very few aggregates, the modified clusters are much better distributed and dispersed in the organic matrix than they are for the higher Ti contents. Moreover, the incorporation of a higher content of Ti clusters into a dimethacrylate matrix broadens the size distribution and therefore decreases the homogeneity of nanomaterials. Figures 6a and 6b show the bright field TEM and energy-filtered micrographs for the UV_Ti19.2 sample. The number of titanium-enriched domains has significantly increased. Now, the titanium clusters aggregates are

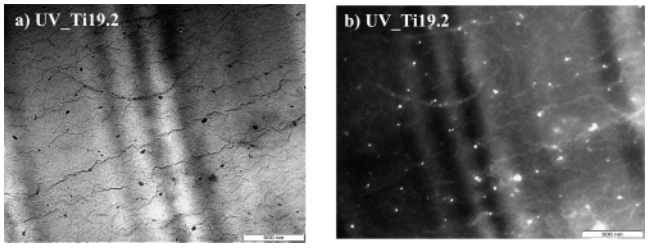

Figure 6. (a) Bright field TEM images and (b) filtered energy image of UV_Ti19.2 with bar scale of 500 nm.

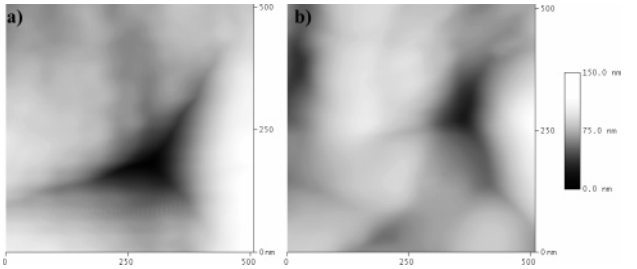

Figure 7. Comparison of the indent dimensions derived from height images using NanoMc software between (a) the pure matrix UV_CDHEMA and (b) UV_Ti2.5 for a scan size of 507 × 507 nm^2 and a trigger threshold of 2.5 V.

Table 4. Indent Parameters of UV_CDHEMA and UV_Ti2.5 Determined with NanoMc Software[37]

sample name	depth h [nm]	projected area A_P [μm^2]	surface area A_S [μm^2]
UV_CDHEMA	115.4	0.14	0.17
UV_Ti2.5	89	0.06	0.12
error bar	±5	±0.01	±0.01

denser and more compact. The power law exponent $P_1 = 3.26$ extracted from SAXS fitting profile reveals this effect, too. Both TEM and SAXS results indicate the presence of surface fractals in the system, i.e., compact and dense particles with rough surfaces, rather than a mass fractal. Unexpectedly, despite the incorporation of a very high content of 19.2 wt % titanium clusters into UV_HEMA matrix, the size of the compact particles does not exceed 60 nm (Figure 6), whereas, for UV_Ti5 and UV_Ti7.5, relatively large aggregates up to 180 nm have been measured. There are two possible explanations for this different behavior between the two matrixes. First, the reaction kinetics and the extent of cross-linking in the two matrixes is very different, and this may have an influential impact on the aggregation process. Second, the interactions between the matrix and the Ti clusters are also different, with the UV_HEMA matrix being more compatible with the nanoclusters, thus leading to better dispersion and smaller sizes for the aggregates. However, at present, it is still unclear which of the two scenarios is the most dominant one.

3.3. Enhancement of Thermomechanical and Thermal Properties. 3.3.1. Nano-indentation for Hardness Assessment. Height images of the indents for the samples UV_CDHEMA and UV_Ti2.5 are given in Figure 7. Because the hardness of each sample can be estimated by the measurement of the size of the indent, NanoMc[37] software has been used to determine the indent dimensions such as the depth, the surface, and the projected area shown in Table 4. By incorporating the titanium clusters into the pure organic matrix, we found that all indent dimensions decreased. This

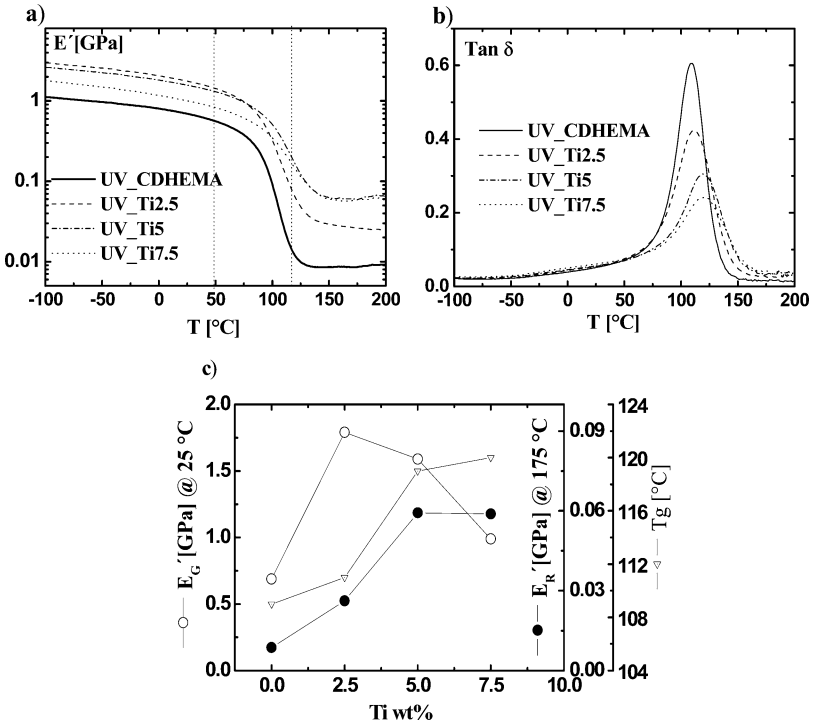

Figure 8. DMA curves of UV_CDHEMA, UV_Ti2.5, UV_Ti5, and UV_Ti7.5 taken at the final run. (a) Dynamic storage moduli E'[GPa], (b) loss factor tan δ. (c) Storage modulus below the T_g, $E_{G'}$ at 25 °C (the left axis), above the T_g, $E_{R'}$ at 175 °C (right axis) and the glass temperature T_g (at most right axis) as a function of the titanium clusters weight incorporated into the dimethacrylate matrix.

qualitative estimation enables us to conclude that the titanium clusters play a significant role in increasing the hardness of the material.

3.3.2. Dynamic Mechanical Thermal Properties of Dimethacrylate/Titanium Clusters-Based Nanomaterials. Storage moduli E' and loss factors tan δ have been measured as a function of temperature for the neat matrix UV_CDHEMA and for the hybrids UV_Ti2.5, UV_Ti5, and UV_Ti7.5. The UV_Ti19.2 sample was very brittle, and as a result, DMA measurements could not be carried out. Figure8a and b illustrate the storage modulus E' and the loss factor tan δ as a function of temperature. Over the whole temperature range -100 °C $\leq T \leq$ 200 °C, all hybrids show a much higher storage modulus than that of the neat matrix. In addition, the glass transition temperature (i.e., α relaxation) has shifted from 109.6 °C for the neat matrix UV_CDHEMA to 120 °C for the UV_Ti7.5 sample (Figure 8b). Figure 8c shows the variation of the storage modulus E' versus the titanium cluster content at two temperatures, below T_g at $T = 25$ °C and above T_g at $T = 175$ °C. The different behaviors that have been found in the glassy regime and in the rubbery may be seen in Figure 8c. There are, however, a number of interesting observations seen in Figure (8a,c). First, there appears to be a maximum in terms of storage modulus for the lowest Ti content (Ti_2.5%) hybrid in the glassy regime (i.e., below T_g). In fact, the stiffness of the matrix increases by a factor of 2.5 just with incorporating only 2.5% Ti clusters inside it. The increase of the Ti content does not lead to an increase in the hybrids' stiffness. On the contrary, it leads to a mild and a clear decrease for the Ti_5% and Ti_7.5% hybrids compared to that of the Ti_2.5%, respectively. On the other hand, the scenario is different and much closer to what one might have expected for the rubbery regime (i.e., above T_g). In this case, the higher Ti content hybrids exhibit a higher storage modulus, but it may also be seen from Figures 8a and 8c that, practically, there is little difference between the Ti_5% and the Ti_7.5% hybrids. It is noteworthy that the addition of 2.5% of Ti leads to an increase of the stiffness in the rubbery regime by a factor of 3, while in the case of 5 and 7.5% Ti content samples, the increase is by a factor of 7. Interestingly enough, the system reaches a sort of a saturation level above 5% of Ti content for the stiffness in the rubbery regime. The behavior of the systems above T_g may be explained through the change of the cross-linking density with the incorporation of the Ti clusters in the matrix. As the cross-linking density increases in the system because of the addition of the nanoclusters, the storage modulus also increases above T_g as predicted by theory.[38] Remarkably, there is no further increase of E'_R from 5 wt % to 7.5 wt % titanium cluster content. It appears that, above a critical concentration of Ti clusters, there is no further increase in the effective cross-linking density. This may be due to the fact that, because of the higher degree of aggregation in the high content Ti samples, there are potentially other mechanisms (such as self-reaction, steric hindrance, etc.) that hinder any further incorporation of the nanoclusters in the polymer network, thus causing the effective cross-linking density to reach a maximum value.

The glass transition temperature T_g shows a comparable trend, albeit a far less pronounced trend, than that of the E'_R (Figure 8b). The increase of the T_g generally reflects a restriction in the segmental chain mobility because of the cross-linking effect. It is surprising, however, that the E'_R increases by a factor of 3, while the T_g increases by about 2 °C with the addition of only 2.5% Ti clusters in the system. On the other hand, for the 5 and 7.5 Ti wt %, the increase in the E'_R and T_g is practically of the same order. The comparison between the T_g and E'_R results indicates that, in the case of the

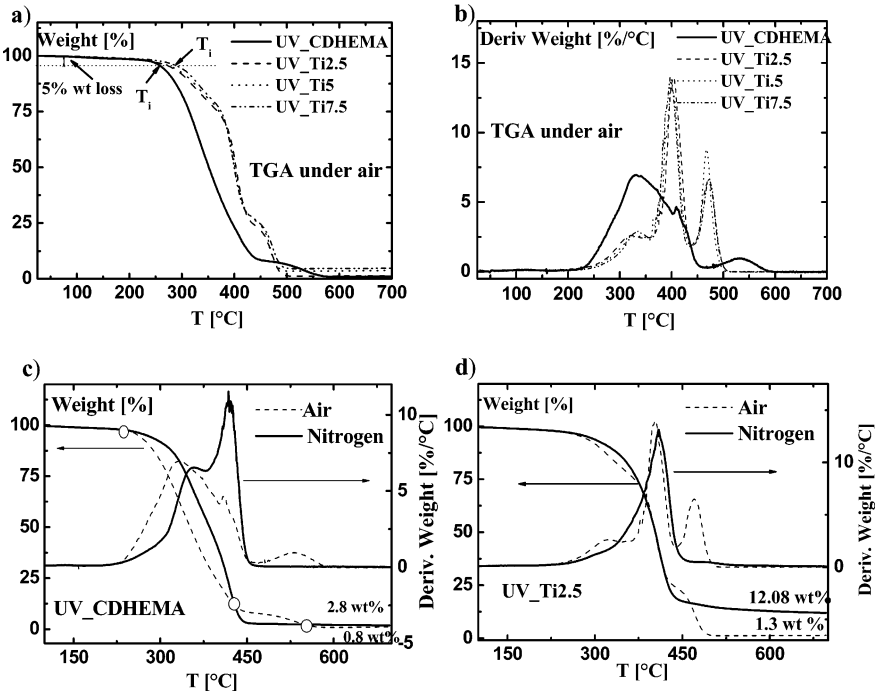

Figure 9. (a) Weight loss and (b) derivative thermographs DTGA curves of the neat matrix UV_CDHEMA and hybrid nanomaterials UV_Ti2.5, UV_Ti5, and UV_Ti7.5 under air atmosphere. TGA and DTGA curves under air and under nitrogen for (c) the neat matrix and (d) UV_Ti2.5.

Table 5. TGA Results under Air Atmosphere

TGA under air atmosphere							
UV_CDHEMA		UV_Ti2.5		UV_Ti5.0		UV_Ti7.5	
T_{max} [°C]	weight loss [%]	T_{max} [°C]	weight loss [%]	T_{max} [°C]	weight loss [%]	T_{max} [°C]	weight loss [%]
332	72.4	324	19.3	332	21.9	335	19.9
409	18.5	403	56.6	400	52.6	397	52.7
531	7.5	471	22.8	468	22.9	472	22.7

Table 6. TGA Results under N_2 Atmosphere

TGA under N_2 atmosphere							
UV_CDHEMA		UV_Ti2.5		UV_Ti5.0		UV_Ti7.5	
T_{max} [°C]	weight loss [%]	T_{max} [°C]	weight loss [%]	T_{max} [°C]	weight loss [%]	T_{max} [°C]	weight loss [%]
358	46.4	409	84.0	405	80.1	401	78.3
418	50.8	495	3.7	475	4.9	468	5.0

UV_Ti2.5 sample, there might be other than the cross-linking density mechanisms responsible for the increase in stiffness, such as the degree of dispersion, physical interactions between the clusters and the polymer chains, etc. It is, however, very difficult to deconvolute the effect of these mechanisms, given the fact that the polymer network is very heterogeneous from its nature. The loss tangent maximum $(\tan \delta)_{max}$ has been found to decrease with the titanium clusters content (Figure 8b). However, UV_Ti2.5 still exhibits a damping factor of $\tan \delta = 0.4$. Usually, polymeric materials with $\tan \delta > 0.3$ are considered as having very good damping properties.[39] The broadening of the glass transition peak ΔT, determined from the full width at half-maximum of the loss factor peak, is linked to the distribution of mobility (i.e. relaxation times) of polymer segments.[40] Subsequently, ΔT may be taken as a measure of the structural heterogeneity degree of the network. Values for ΔT obtained from Figure 8b are 30 °C for UV_CDHEMA, 42 °C for UV_Ti2.5, 48 °C for UV_Ti5, and 57 °C for UV_Ti7.5. The increase of ΔT indicates that the hybrids are more heterogeneous than the neat matrix, and that the degree of heterogeneity increases with the increase of the titanium cluster content.

3.3.3. Thermal Stability of Nanomaterials. Figure 9a illustrates the TGA thermographs of weight loss as a function of the temperature under air atmosphere, and Figure 9b shows its derivative DTGA. Tables 5 and 6 summarize the weight loss at each degradation step and the corresponding peak decomposition temperature T_{max} under air and nitrogen atmospheres, respectively. Unexpectedly, the TGA curves of the hybrids are very different from that of the neat resin. A comparison of the initial decomposition temperature (T_i), defined as 5% weight loss in Figure 9a, shows that the main degradation process under air atmosphere in the case of hybrids starts about 20 °C higher than in the neat matrix. On the other hand, the peak decomposition temperature, underlined in Table 6 and corresponding to the major weight-loss step under air is shifted significantly from $T_{max} = 332$ °C for the neat matrix to approximately 400 °C for hybrids because of the pres-

ence of the clusters. Furthermore, the increase of the titanium content from 2.5 to 7.5 wt % does not alter the initial degradation temperature (T_i) (Figure 9a) and the peak decomposition temperature (Figure 9b, Table 5). TGA curves under air and under nitrogen atmosphere are displayed for UV_CDHEMA and UV_Ti2.5 in Figure 9c and d. Three distinct stages of degradation are observed under air atmosphere, while only two stages are observed under nitrogen. Obviously, the third decomposition peak under air atmosphere located at a temperature above 430 °C (see derivatives in Figure (9c,9d)) originates from the weight loss through a pure oxidation reaction. However, below 430 °C, some oxidative degradation in the experiments under air atmosphere is probably also present in combination with other degradation mechanisms. For the temperature range between 245 and 430 °C, the weight loss curve under air of the neat matrix lies below the one measured under nitrogen atmosphere (Figure 9c), indicating faster degradation that one also might expect in the presence of O_2. The difference in weight loss at constant temperature (in the range 245−430 °C) is on the order of 20 wt % for the neat matrix. On the other hand, for the UV_Ti2.5 sample, a very small difference in weight loss has been detected (Figure 9d) between the experiments done under air and N_2 atmospheres. Therefore, even with a small amount of modified-titanium clusters, one may stabilize and protect the neat matrix against oxidative degradation. For the hybrids UV_Ti2.5, UV_Ti5, and UV_Ti7.5, the peak decomposition temperatures corresponding to the major degradation weight loss under oxygen and nitrogen atmospheres (values of T_{max} underlined in Tables 5 and 6) are only slightly different. T_{max} varies from 403 to 397 °C under air (Table 5) and from 409 to 401 °C under nitrogen (Table 6), while the titanium content increases from 2.5 to 7.5 wt %. Additionally, the initial degradation temperature (T_i) (defined as 5% weight loss in Figure 9a), varies from 280 to 285 °C under air and from 288 to 290 °C under nitrogen. Hence, one may conclude that the increased thermal stability of the hybrid materials is mainly due to the antioxidant activity of titanium clusters because titanium−oxo-species are well-known by their ability to trap efficiently the electrons and to generate Ti^{3+}. Such reduced species have been detected by electron spin resonance (ESR).[41,42] It is, however, noteworthy to note that the matrix exhibits two distinct peaks (Figure 9c) of decomposition under N_2, which may be associated with chain scission and depolymerization, but the hybrids exhibit only one peak at the same conditions (Figure 9d). Hence, it appears that the Ti clusters also stabilize the polymer network in addition to the antioxidation protection they offer to the matrix.

The oxidative degradation of polymers is a radical reaction, which proceeds by a free-chain mechanism consisting of three important steps: initiation, propagation, and termination.[43] It should be noted that extremely long lifetimes of trapped radicals at room temperature have been observed using electron spin resonance ESR with photopolymerized dimethycrylate matrixes[44,45] similar to the neat organic matrix UV_CDHEMA used in the present study. It has also been observed by ESR that oxygen reacts rapidly with these trapped radicals, although no peroxy radicals ($ROO^{\bullet}$) could be detected because of their fast transformation to hydroperoxides (ROOH).[46] The elevated weight loss due to the oxidative reaction in the neat matrix is likely to be related to the presence of a high amount of such trapped radicals. Titanium clusters may inhibit the oxidative degradation either by transforming the hydroperoxides (ROOH) into nonradical yielding compounds, or by acting as chain-breaking antioxidants via hydrogen-donating mechanisms, i.e., scavenging of the C-centered alkyl ($R^{\bullet}$) or the O-centered ($RO^{\bullet}$, $RO_2^{\bullet}$) radicals formed in the initiation and propagation steps of the oxidative degradation reaction.[43,47] It appears that, at higher temperatures, the octa-functional HEMA-modified titanium clusters react efficiently with the remaining free radicals entrapped in the photopolymerized dimethacrylate network and/or with the radicals formed during the different stages of the oxidative process. Such a reaction may explain the antioxidant effect due to the presence of the titanium clusters in hybrid nanomaterials.

The residue weight under nitrogen for $T > 600$ °C of the neat matrix is 2.8 wt %. This indicates that the fragment products of the degradation are volatile. In the absence of oxidation, such an effect is known to happen when the thermal degradation mechanism proceeds by random chain scission. Nevertheless carbonization mechanisms have been demonstrated to occur to some extent for aromatic-based polymers such as the matrix used in the present study. For the UV_Ti2.5, the residue weight under nitrogen is about 12 wt %. This result, in conjunction with the fact that, under N_2, the hybrids exhibit only one decomposition peak as discussed previously, clearly demonstrates that the presence of the Ti clusters inside the polymer network increases the stability of the network and reduces degradation through depolymerization and chain scission, while favoring carbonization mechanisms.

Conclusions

HEMA-modified titanium clusters have been incorporated into two different organic matrixes: dimethacrylate-HEMA, which is a highly cross-linked and spatially heterogeneous network, and poly(HEMA), which forms a linear network, resulting in the manufacturing of novel hybrid materials.

SAXS and TEM experiments have shown that the best dispersion is achieved with a low content of Ti clusters (2.5 wt %), and the clusters aggregate to form larger structures of about 30 nm in size. The analysis of the SAXS results with the Beaucage model in the case of the dimethacrylate matrix revealed that the titanium cluster aggregates are formed following a reaction-limited cluster−cluster aggregation growth process (RLCA). These aggregates are built up from correlated subunits with approximately the size of one single cluster. According to the SAXS results, the variation of the titanium clusters content does not significantly change the ramified structure of the aggregates in the first system. By increasing the Ti content, the size and distribution of the cluster aggregates increased significantly to about 180 nm, while there were still a few smaller-size aggregates present in the system.

SAXS, TEM, and EFTEM analyses for a higher titanium cluster content of 19.2 wt % incorporated into un-cross-linked poly(HEMA) indicate the formation of compact, highly dense and well-distributed aggregates with a size of $\approx$ 50 nm. In this case, correlation effects strongly increased compared to that of the materials with a lower titanium cluster loading incorporated into dimethacrylate matrixes, as was revealed through

SAXS. In a comparison, the titanium cluster structures of 19.2 wt % into HEMA monomer before and after UV curing, an increase of the short-range order was detected.

Dynamic mechanical analysis revealed a significant reinforcement effect through the incorporation of the modified titanium clusters into the dimethacrylate matrix. The increase of the titanium content in the dimethacrylate matrix influences differently the storage moduli in the glassy regime E'_G and in the rubbery regime E'_R. It was found that, with only 2.5 wt % of Ti clusters, the E'_G increased by a factor of 2.5 and the E'_R increased by a factor of 3, while the T_g only slightly increased by 2 °C. At the same time, the maximum of the damping factor tan δ only slightly decreased from 0.6 to 0.4, thus indicating that the 2.5 wt % Ti hybrid still retains excellent damping properties. In addition to the significant increase of the matrix stiffness, the incorporation of the Ti cluster lead to a remarkable enhancement in the thermal stability (an increase by 70 °C in the main degradation temperature) of the system, again at very low content of Ti (2.5 wt %). The increase in the thermal stability is due to two possible mechanisms: the elimination of free radicals that propagate the oxidative reaction, and the stabilization of the polymer network to shift chain scission and depolymerization reactions at higher temperatures. The addition of titanium clusters with 2.5 wt % Ti into the organic medium also lead to a significant increase in hardness, which manifested itself in the nano-indentation tests. Thus, through the incorporation of a low content of modified Ti clusters, hybrid materials with enhanced mechanical and thermal properties may be manufactured.

Acknowledgment. The authors would like to acknowledge financial support by the European Union (RTN project NBB-HYBRIDS, contract number HPRN-CT-2002-00306). We would also like to acknowledge the help of Mr. Torsten Hofmann with the SAXS measurements and of Dr. Martin Bauer in fitting the SAXS profiles.

References and Notes

(1) *Functional Hybrid Materials*, Gómez-Romero, P., Sanchez, C, Eds.; Wiley-VCH: Weinheim, 2004.
(2) Novak, B. M. *Adv. Mater*. **1993**, *5*, 422.
(3) Sanchez, C.; Ribot, F. *New. J. Chem*. **1994**, *18*, 1007.
(4) Wojcik, A. B.; Klein, L. C. *Appl. Organomet. Chem*. **1997**, *11*, 129.
(5) Shea, K. J.; Loy, D. A. *Chem. Mater*. **2001**, *13*, 3306.
(6) Schubert, U. *J. Sol.−Gel Sci. Technol*. **2003**, *26*, 47.
(7) Livage, J.; Henry, M.; Sanchez, C. *Prog. Solid State Chem.* **1988**, *18*, 259.
(8) Brinker, C. J.; Scherrer, G. W. *Sol−Gel Science: The Physics and Chemistry of Sol−Gel Processing*; Academic Press: San Diego, 1990.
(9) Sanchez, C.; Lebeau, B.; Chaput, F.; Boilot, J. P. *Adv. Mater.* **2003**, *15*, 1969.
(10) Sanchez, C.; Soler-Illia; Riot, F.; Lalot, T.; Mayer, C. R.; Cabuil, V. *Chem. Mater.* **2001**, *13*, 3061.
(11) Schubert, U. *Chem. Mater*. **2001**, *13*, 3487.
(12) Kickelbick, G. *Prog. Polym. Sci*. **2003**, *28*, 83.
(13) Cook, W. D. *J. Appl. Polym. Sci*. **1991**, *42*, 1259.
(14) Gao, F.; Tong, Y.; Schricker, S. R.; Culbertson, B. M. *Polym. Adv. Technol*. **2001**, *12*, 355.
(15) Fornasieri, G.; Rozes, L.; Le Calvé, S.; Alonso, B.; Massiot, D.; Rager, M. N.; Evain, M.; Boubekeur, K.; Sanchez, C. *J. Am. Chem. Soc.* **2005**, *127*, 4869.
(16) Bocchini, S.; Fornasieri, G.; Rozes, L.; Trabelsi, S.; Galy, J.; Zafeiropoulos, N. E.; Stamm, M.; Gérard, J. F.; Sanchez, C. *Chem. Commun.* **2005**, 2600.
(17) Beaucage, G.; Schaefer, D. W. *J. Non-Cryst. Solids* **1994**, *172−174*, 797.
(18) Beaucage, G. *J. Appl. Crystallogr.* **1995**, *28*, 717.
(19) Beaucage, G. *J. Appl. Crystallogr.* **1996**, *28*, 134.
(20) Avnir, D. *Fractal Approach to Heterogeneous Chemistry*, Avnir, D., Ed.; John Wiley & Sons: New York, 1989; p 131−160.
(21) Schaefer, D. W. *Mater. Res. Soc. Symp. Proc.* **1987**, *79*, 47.
(22) Schaefer, D. W. *MRS Bull.* **1988**, *8*, 22.
(23) Beaucage, G.; Ulibari, T. A.; Black, E. P.; Schaefer, D. W. In *Hybrid Organic−Inorganic Composites*; ACS Symposium Series 585; American Chemical Society: Washington DC, 1995; p 97.
(24) Born, M.; Green, H. S. *Proc. R. Soc. London* **1946**, *A188*, 10.
(25) Fournet, G. *Compt. Rend.* **1949**, *228*, 1801.
(26) Fournet, G. *Acta Crystallogr*. **1951**, *4*, 293.
(27) Guinier, A.; Fournet, G. *Small-Angle Scattering of X-rays*; Wiley: NewYork, 1955; p 40−70.
(28) Porod, G. *Kolloid-Z*. **1951**, *124*, 83.
(29) Lin, M. Y.; Lindsay, H. M.; Weitz, D. A.; Ball, R. C.; Klein, R.; Meakin, P. *Phys. Rev. A* **1990**, *41*, 2005.
(30) Mosset, A.; Galy, J. *C. R. Acad. Sci. Paris, Ser. II* **1988**, *307*, 1747.
(31) Bowman, C. N.; Peppas, N. A. *J. Appl. Polym. Sci.* **1991**, *42*, 2013.
(32) Simon, G. P.; Allen, P. E. M.; Bennett, D. R. G.; Williams, E. H. *Macromolecules* **1989**, *22*, 3555.
(33) Schaefer, D. W.; Martin, J. E.; Keefer, K. D. In *Physics of Finely Divided Matter*; Boccara, N., Daoud, M., Eds.; Springer-Verlag: New York, 1985, p 33.
(34) Rey, L.; Galy, J.; Sautereau, H. *Macromolecules* **2000**, *33*, 6780.
(35) Rey, L.; Duchet, J.; Galy, J.; Sautereau, H.; Vouagner, D.; Carrion, L. *Polymer* **2002**, *43*, 4375.
(36) Dusek, K.; Plestil, J.; Lednicky, F.; Lunak, S. *Polymer* **1978**, *19*, 393.
(37) Shuman, D. *NanoMc*, version 3.1; www.nanomc.com; NanoMc: Wappingers Falls, NY.
(38) Flory, P. J. *Principles of Polymer Chemistry*; Cornell University Press: Ithaca, NY, 1953.
(39) Li, F.; Perrenoud, A.; Larock, R. C. *Polymer* **2001**, *42*, 10133.
(40) Matsuoka, S. *Relaxation Phenomena in Polymers*; Hanser Publishers: New York, 1992.
(41) Soppera, O. Thesis, University de Haute Alsace, 2003.
(42) Kameneva, O.; Kuznetsov, A. I.; Smirnova, L. A.; Rozes, L.; Sanchez, C.; Alexandrov, A.; Chhor, K.; Kanaev, A. *J. Mater. Chem.* Submitted.
(43) Kamiya, Y.; Niki, E. Oxidative Degradation. In *Aspects of Degradation and Stabilization of Polymers*; Jellinek, H. H. G., Ed.; Elsevier/North-Holland: New York, 1978; p 79.
(44) Kloosterboer, J. G.; Van de Hei, G. M. M.; Gossink, R. G.; Dortand, G. C. M. *Polym. Commun.* **1984**, *25*, 322.
(45) Kloosterboer, J. G.; Van de Hei, G. M. M.; Lijten, G. G. C. M. 1986 In *Integration of Fundamental Polymer Science and Technology*; Kleintjens, L. A., Lemstra, P. J., Eds.; Elsevier Applied Science: London, 1986; p 198.
(46) Best, M. E.; Kasai, P. H. *Macromelcules* **1989**, *22*, 2622.
(47) Pospisil, J. Antioxidants. In *Degradation and Stabilization of Polymers*; Jellinek, H. H. G., Ed.; Elsevier: Amsterdam, 1983; p 193.

MA0507239